Ab Initio/Density Functional Theory and Multichannel RRKM Calculations for the CH_3O + CO Reaction

Baoshan Wang,* Hua Hou, and Yueshu Gu

School of Chemistry, Shandong University, Jinan 250100, P. R. China

Received: April 9, 1999; In Final Form: June 14, 1999

The potential energy surface for the reaction of methoxy radical with carbon monoxide has been studied using the G2(B3LYP/MP2/CC) method. Two reaction mechanisms were revealed. The hydrogen abstraction of CH_3O by CO produces CH_2O + HCO via a barrier of 24.19 kcal/mol. The addition of CH_3O to CO proceeds to an intermediate CH_3OCO via a barrier of 6.39 kcal/mol. The products, CH_3 and CO_2, can be formed in two ways. One is the C−O bond cleavage of the CH_3OCO radical. The other involves the isomerization of CH_3OCO to the CH_3CO_2 radical and the subsequent C−C bond fission. CH_2O and HCO can be formed via the path $CH_3OCO \rightarrow$ TS6 $\rightarrow$ IM4 $\rightarrow$ TS7 $\rightarrow$ CH_2O + HCO. A radical product, CH_2COOH, is formed through the hydrogen rearrangement of the CH_3CO_2 radical. Multichannel RRKM calculations have been carried out for the total and individual rate constants for various channels over a wide range of temperatures and pressures using the ab initio data. At lower temperatures, the title reaction is dominated by the stabilization of the CH_3OCO radical. At higher temperatures, the CH_3 + CO product channel and the direct hydrogen abstraction channels become dominant and competitive. The title reaction shows the typical falloff behavior. The calculations were compared with the available experimental data.

I. Introduction

The methoxy radical (CH_3O) is an important intermediate in the photochemical oxidation of hydrocarbons in the atmosphere,[1−3] and it may play a role in the conversion of NO to NO_2 in polluted urban atmosphere.[4] The study of the reactions of CH_3O radicals with other atmospheric gases is of considerable interest. One of the most important reactions is CH_3O + CO, which is analogous to the well-known reaction of OH + CO.[5,6] The CH_3O + CO reaction is also an important process in methane combustion.[7]

Experimentally, Lissi et al.[8] studied the CH_3O + CO reaction over the temperature range 396−426 K and derived the Arrhenius expression as $k = 2.6 \times 10^{-11}\exp(-5940/T)$. The products CO_2, CH_2O, CH_3OH, and C_2H_6 were observed. The authors noted that the mechanism to describe these products could only be rationalized by a free radical chain reaction. However, Wiebe et al.[9] found that the principal product of the CH_3O + CO reaction is $(CH_3O)_2CO$ or $(CH_3OCO)_2$ instead of CO_2. Moreover, the rate for the CH_3O + CO reaction was suggested to be essentially temperature-independent at 298, 353, and 423 K. Sander et al.[10] showed that the room-temperature rate of removal of CH_3O radicals by CO was very slow with an upper limit of 8.32×10^{-15} cm^3 molecule^{-1} s^{-1}. Wantuck et al.[11] examined the CH_3O + CO reaction over an extended temperature range from 473 to 973 K by the laser-induced fluorescence (LIF) technique. The rate was observed to exhibit nonlinear Arrhenius behavior above 773 K.

Theoretically, although the analogous reaction OH + CO has been understood extensively, the CH_3O + CO reaction has not been well established up to now. In the study of the $C_2H_3 + O_2$ reaction by Lin et al.,[12] some relevant species of the CH_3O + CO reaction were optimized by coincidence. Very recently, Francisco[13] studied the CH_3O + CO reaction by ab initio molecular orbital theory. At the MP2 and QCISD(T) levels of theory, only one addition−elimination path, i.e., CH_3O + CO $\rightarrow$ $CH_3OCO \rightarrow CH_3 + CO_2$, was found. Unfortunately, as will be illustrated below, this mechanism is wrong because the transition state involved was identified incorrectly.

Obviously, no conclusive result can be obtained from the previous experiments and calculations. To understand this important reaction, several issues need to be clarified: What is the reaction mechanism involved? What are the dominant products? What is the dependence of the reaction rate constants and branching ratios on the temperature and pressure? To address these questions, we carried out a detailed ab initio/density functional study of nearly all possible channels of the title reaction including the consideration of various intermediates for the first time. The high-quality potential energy surface was obtained at the G2(B3LYP/MP2/CC)[14] level. The ab initio data were employed for the RRKM calculations of the multichannel rate constants over a wide range of temperatures and pressures. Our goal is to quantify the CH_3O + CO reaction theoretically in order to elucidate the reaction mechanism and to provide a reliable estimate of the rate constants for practical atmospheric and combustion applications.

II. Computation

The geometries of all the reactants, products, various intermediates, and transition states for the CH_3O + CO reaction have been optimized using the unrestricted hybrid density functional UB3LYP method, i.e., Becke's three-parameter nonlocal-exchange functional[15] with the nonlocal correlation functional of Lee, Yang, and Parr,[16] with the 6-31G(d) basis set. Vibrational frequencies, calculated at the UB3LYP/6-31G(d) level, have been used for characterization of stationary points, zero-point energy (ZPE) correction, and RRKM computations. All the

* Corresponding author. E-mail: guojz@icm.sdu.edu.cn.

10.1021/jp991203g CCC: $18.00
Published on Web 09/18/1999

TABLE 1: Overall Moments of Inertia, Reduced Moments of Inertia for the Free Internal Rotor, and Vibrational Frequencies (Unscaled) for Various Species Involved in the $CH_3O + CO$ Reaction

species	I_a, I_b, I_c[a]	I_r[b]	frequencies[c]
CH_3O	11.49, 64.92, 65.33		758, 979, 1126, 1400, 1401, 1549, 2923, 2989, 3025
CO	31.7		2210
IM1	30.87, 385.59, 404.91	10.7	35, 217, 316, 615, 1004, 1135, 1182, 1231, 1494, 1521, 1525, 1886, 3075, 3154, 3187
IM1′	30.21, 387.47, 406.16	10.8	30, 235, 330, 620, 998, 1130, 1188, 1252, 1490, 1516, 1532, 1883, 3073, 3161, 3164
IM2	136.05, 196.37, 321.12	10.4	39, 392, 543, 569, 905, 1004, 1070, 1179, 1412, 1487, 1495, 1607, 3067, 3193, 3163
IM3	158.56, 170.46, 329.02		233, 438, 443, 596, 604, 725, 910, 992, 1215, 1339, 1491, 1722, 3175, 3297, 3742
IM3′	158.48, 178.25, 324.27		315i, 366, 518, 591, 621, 897, 1039, 1182, 1334, 1447, 1845, 3173, 3276, 3705
IM3″	154.33, 174.42, 328.75		190, 428, 479, 645, 687, 752, 936, 959, 1163, 1410, 1472, 1691, 3191, 3287, 3746
IM4	31.88, 363.28, 394.71		160, 245, 363, 475, 645, 1023, 1045, 1183, 1272, 1427, 1491, 1875, 3007, 3167, 3324
TS1	43.50, 502.57, 534.36	37.4	265i, 87, 153, 192, 306, 1016, 1135, 1155, 1438, 1446, 1542, 2152, 2981, 3043, 3072
TS2	38.95, 449.44, 476.17	11.6	1277i, 40, 250, 349, 645, 734, 810, 988, 1131, 1456, 1462, 2024, 3122, 3284, 3296
TS2[d]	40.96, 438.46, 467.23		6032i, 68, 260, 441, 748, 757, 880, 982, 1174, 1493, 1496, 2062, 3157, 3331, 3355
TS2[e]	41.20, 448.20, 477.10		2648i, 56, 237, 316, 656, 729, 791, 970, 1111, 1471, 1476, 1996, 3135, 3295, 3314
TS3	76.74, 314.19, 378.96	9.80	942i, 68, 270, 337, 660, 888, 930, 1200, 1293, 1470, 1493, 1924, 3110, 3226, 3268
TS4	152.88, 184.04, 325.30	10.6	246i, 96, 389, 595, 644, 954, 1006, 1107, 1373, 1464, 1502, 1805, 3076, 3172, 3188
TS5	133.05, 195.58, 316.25		2071i, 403, 493, 538, 601, 928, 993, 1043, 1095, 1176, 1430, 1780, 1962, 3142, 3245
TS6	43.80, 334.23, 365.57		2091i, 213, 480, 504, 721, 916, 1018, 1138, 1186, 1186, 1487, 1880, 1938, 3132, 3250
TS7	45.90, 449.71, 476.09	35.7	517i, 92, 229, 289, 422, 742, 970, 1121, 1241, 1449, 1616, 1916, 2770, 3011, 3100
TS8	82.82, 550.54, 620.86	11.4	1770i, 37, 79, 356, 398, 447, 973, 1081, 1237, 1306, 1480, 1626, 2080, 2885, 2943
CH_3	6.33, 6.33, 12.66		454, 1431, 1431, 3142, 3316, 3316
CO_2	156.15		640, 640, 1372, 2436
CH_2O	6.33, 46.72, 53.05		1198, 1279, 1563, 1848, 2917, 2968
HCO	2.59, 40.6, 43.19		1130, 1946, 2663
CH_2CO	6.34, 177.16, 183.50		440, 538, 592, 1003, 1180, 1435, 2240, 3208, 3297
OH	3.27		3643

[a] In amu. [b] In amu. [c] In cm^{-1}. i represents imaginary frequency. [d] At the MP2(full)/6-31G(d) level. [e] At the QCISD/6-31G(d) level.

stationary points have been positively identified for the minimum (number of imaginary frequencies NIMAG = 0) or transition state (NIMAG = 1). Connections of the transition states between designated reactants and products have been confirmed by intrinsic reaction coordinate (IRC) calculations.[17] Since UHF wave functions are not spin eigenfunctions, we monitored the expectation values of $\langle S^2 \rangle$. For doublets, $\langle S^2 \rangle$ was always in the range 0.750−0.777, where 0.750 is the exact value. Thus, spin contamination is not severe.

To obtain more reliable energies, we used the G2(B3LYP/MP2/CC) method,[14] which is a modification of the Gaussian-2 (G2) approach[18] by Pople and co-workers. The method uses B3LYP/6-31G(d) optimized geometries and ZPE corrections (scaled by a factor of 0.98 to eliminate the known systematic errors) and substitutes the QCISD(T)/6-311G(d,p) calculation of the original G2(MP2) scheme for the coupled cluster CCSD(T)/6-311G(d,p) calculation. The total energy in G2(B3LYP/MP2/CC) is calculated as follows:

$$E[\text{G2(B3LYP/MP2/CC)}] = E(\text{CCSD(T)/6-311G(d,p)}] + E[\text{MP2/6-311+G(3df,2p)}] - E[\text{MP2/6-311G(d,p)}] + \Delta E(\text{HLC}) + \text{ZPE}$$

and the empirical "higher level correction" is

$$\Delta E(\text{HLC}) = -0.00451 n_\beta - 0.00019 n_\alpha$$

where n_α and n_β are the number of α and β valence electrons, respectively. It has been shown that molecular energies calculated by the G2(B3LYP/MP2/CC) method have a chemical accuracy of ±2.0 kcal/mol.[14] The Gaussian 94 programs[19] were used for the potential energy surface computations.

Multichannel Rice−Ramsperger−Kassel−Marcus (RRKM) calculations have been carried out for the total and individual rate constants and the branching ratios for various product channels using the method developed by Lin et al.[20−22] with extensive modifications.

III. Results and Discussion

The optimized structures of the reactants, products, intermediates, and transition states are shown in Figure 1. The profile of the potential energy surface for the $CH_3O + CO$ reaction is depicted in Figure 2 in order to clarify the reaction mechanism. The vibrational frequencies and the moments of inertia for various species involved in the $CH_3O + CO$ reaction are listed in Table 1. The total energies and the relative energies for various species are summarized in Table 2. The calculated reaction heats for the channels $CH_3 + CO_2$, $CH_2O + HCO$, and $OH + CH_2CO$ are in good agreement with the experimental values,[23] which implies that the present PES is of high quality and reliable.

1. Potential Energy Surface and Reaction Mechanism. Two kinds of mechanisms for the $CH_3O + CO$ reaction are revealed, as shown in Figure 2. One is the addition−elimination path involving four intermediates (**IM1**−**IM4**) and seven transition states (**TS1**−**TS7**). The other is the direct hydrogen abstraction of CH_3O by CO via the transition state **TS8** leading to the $CH_2O + HCO$ products.

A. Addition−Elimination Mechanism. The reaction of CH_3O with CO starts with the formation of the CH_3OCO radical when the carbon atom in CO attaches itself to the oxygen atom in CH_3O via transition state **TS1**. **TS1** has C_s symmetry and a $^2A'$ electronic state. The forming C−O bond is 2.017 Å, which is 0.16 Å longer than that obtained at the QCISD level by Francisco.[13] This is caused by the flatness of the potential energy surface, as indicated by a small imaginary frequency of 265 cm^{-1}. The other geometrical parameters are similar to those obtained at the QCISD level. The C−O bond distances in the CO molecule and in the CH_3O radical are stretched slightly by 0.005 and 0.022 Å, respectively. The energy of **TS1** is 6.39 kcal/mol higher than that of the reactants $CH_3O + CO$. This barrier height is in agreement with the result of 5.8 kcal/mol obtained by Francisco[13] at the QCISD(T) level with a very large basis set, 6-311++G(3df,3pd).

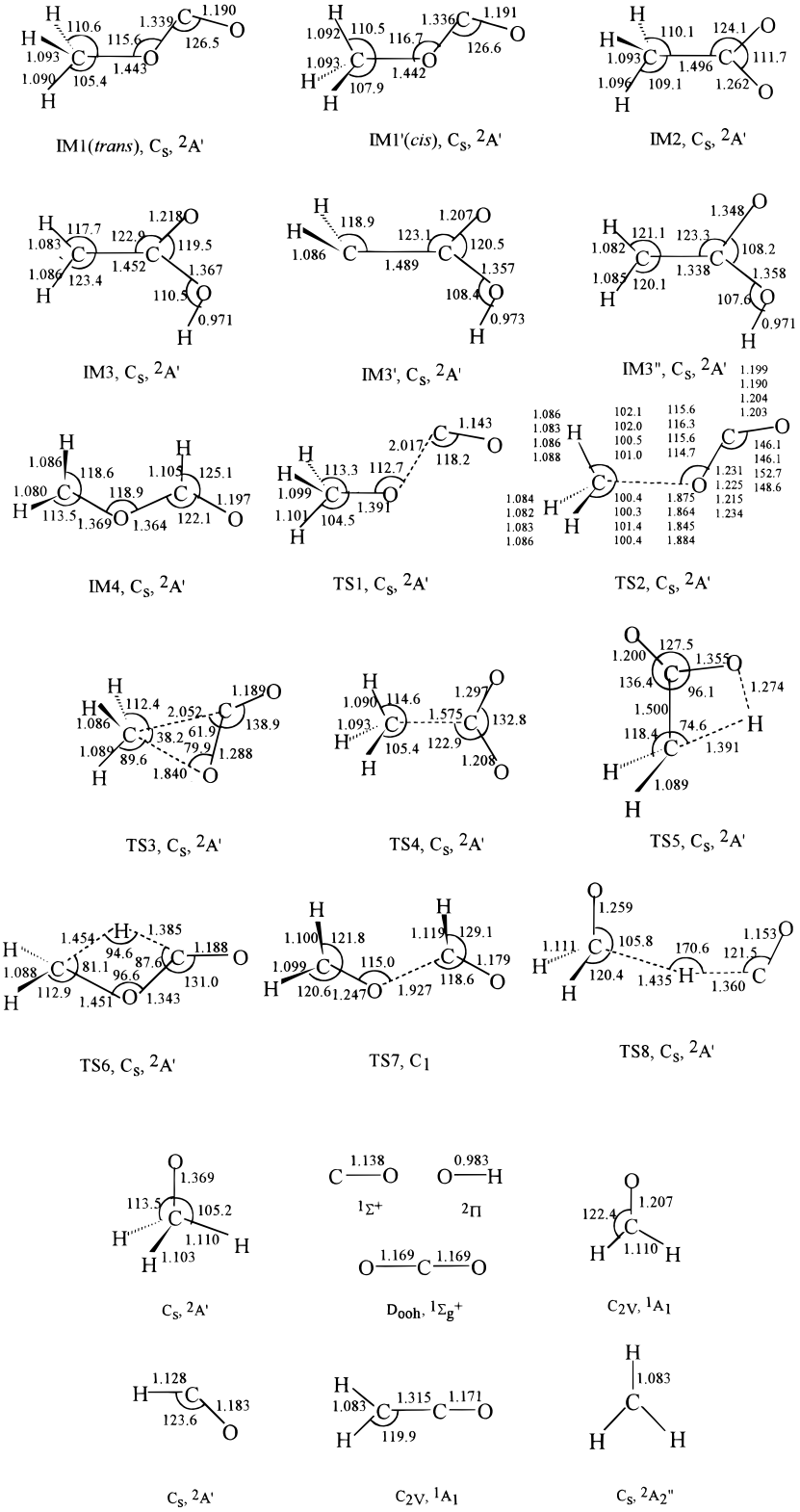

Figure 1. B3LYP/6-31G(d)-optimized geometries of the reactants, products, various intermediates, and transition states for the CH_3O + CO reaction. Bond distances are in angstroms and angles are in degrees. In TS2, from top to bottom, the geometric parameters are optimized at B3LYP/6-31G(d), B3LYP/6-311G(d,p), MP2(full)/6-31G(d), and QCISD/6-31G(d) levels, respectively.

The intermediate CH_3OCO can be created from the reactants in two conformations: **IM1** with the C−H bond in the trans position toward the newly formed O−C bond and **IM1′** with the C−H bond in the cis position. Both **IM1** and **IM1′** have C_s symmetry and $^2A'$ electronic states. **IM1** is only 0.32 kcal/mol more stable than **IM1′** because they have very similar geometries. The exothermicity of CH_3OCO formation at the addition step is calculated to be 14.68−15.00 kcal/mol at the G2(B3LYP/MP2/CC) level.

The subsequent unimolecular decomposition of **IM1** produces CH_3 + CO_2 via transition state **TS2**. The breaking C−O bond in **TS2** is elongated by 0.415 Å. The forming C−O bond is shortened by 0.105 Å, and the angle of O−C−O increases to 146.1°. The barrier height for this process is 31.95 kcal/mol.

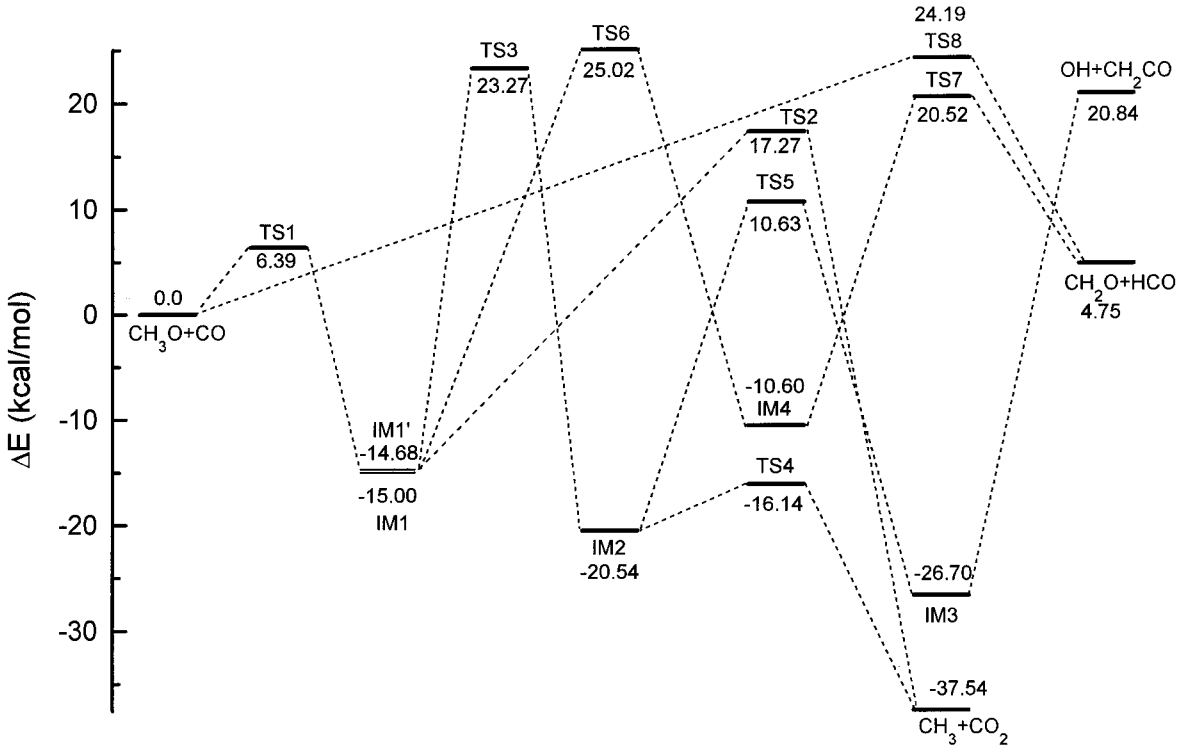

Figure 2. Profile of potential energy surface for the most important channels of the $CH_3O + CO$ reaction.

TABLE 2: Total and Relative Energies for Various Species Involved in the $CH_3O + CO$ Reaction

species	CCSD(T)[a]	MP2[b]	MP2[c]	G2MP2	ΔE[d]	exptl
$CH_3O + CO$	−227.891 435	−227.835 243	−227.967 646	−228.034 737	0.0	0.0
$CH_3 + CO_2$	−227.946 375	−227.906 340	−228.043 224	−228.094 562	−37.54	−36.6
$CH_2O + HCO$	−227.876 148	−227.828 817	−227.967 039	−228.027 161	4.75	5.7
$OH + CH_2CO$	−227.851 740	−227.802 818	−227.939 950	−228.001 522	20.84	20.1
IM1	−227.912 959	−227.867 198	−228.009 164	−228.058 642	−15.00	
IM1′	−227.912 516	−227.866 847	−228.008 800	−228.058 130	−14.68	
IM2	−227.922 342	−227.872 587	−228.012 872	−228.067 469	−20.54	
IM3	−227.927 316	−227.876 326	−228.021 122	−228.077 287	−26.70	
IM3′	−227.919 293	−227.874 043	−228.017 587	−228.068 826	−21.39	
IM3″	−227.868 531	−227.815 958	−227.957 034	−228.014 528	12.68	
IM4	−227.902 161	−227.855 823	−227.999 621	−228.051 632	−10.60	
TS1	−227.882 128	−227.824 191	−227.958 756	−228.024 557	6.39	
TS2	−227.853 272	−227.799 463	−227.945 260	−228.007 215	17.27	
TS3	−227.845 883	−227.789 888	−227.934 725	−227.997 652	23.27	
TS4	−227.915 706	−227.861 842	−228.000 175	−228.060 450	−16.14	
TS5	−227.865 964	−227.813 721	−227.955 695	−228.017 793	10.63	
TS6	−227.843 858	−227.794 014	−227.935 668	−227.994 872	25.02	
TS7	−227.850 758	−227.789 088	−227.930 821	−228.002 033	20.52	
TS8	−227.844 608	−227.779 419	−227.916 896	−227.996 185	24.19	

[a] 6-311G(d,p) basis set. [b] 6-311G(d,p) basis set. [c] 6-311+G(3df,2p) basis set. [d] In kcal/mol. The experimental data are taken from ref 23.

The energy of **TS2** is 17.27 kcal/mol higher than that of the reactants $CH_3O + CO$, which implies that the reaction rate of the formation of CH_3 and CO_2 would be relatively slow and that elimination is the rate-limiting step. Unexpectedly, **TS2** has an abnormally large imaginary frequency, 1277 cm^{-1}, at the B3LYP/6-31G(d) level. It is likely that the CH_3 tunneling may play a role in the decomposition of CH_3OCO. It is interesting to note that the hydrogen tunneling is also found to be dominant in the decomposition of HOCO.[5]

It is surprising that **TS2** has a rather late character for the exothermic **IM1′** → $CH_3 + CO_2$ dissociation and, most of all, significant CH_3 tunneling for such a C−O fission process. We have checked the geometries and vibrational frequencies of **TS2** at the higher levels of theory, that is, at B3LYP/6-311G(d,p), MP2(full)/6-31G(d), and QCISD/6-31G(d). The optimized geometric parameters are shown in Figure 1, and the vibrational frequencies are listed in Table 1. It is obvious that the geometry obtained at the B3LYP/6-31G(d) level are in good agreement with those obtained at the B3LYP/6-311G(d,p) and QCISD/6-31G(d) levels. Moreover, the B3LYP/6-31G(d) vibrational frequencies are in good agreement with the QCISD/6-31G(d) frequencies except that the imaginary vibrational frequency of the former is about 2 times smaller than that of the latter. It is worth noting that the strong CH_3 tunneling is confirmed by the QCISD calculation. However, the MP2-optimized geometry is apparently different from those optimized at the B3LYP and QCISD levels. Meanwhile, there is a very large imaginary frequency, 6032 cm^{-1}, at the UMP2/6-31G(d) level, which must be an artifact of the MP2 calculation. In addition, the spin contamination at the B3LYP level is not severe. The expectation values of $\langle S^2 \rangle$ in the B3LYP/6-31G(d), MP2(full)/6-31G(d), and QCISD/6-31G(d) wave functions are 0.769, 0.894, and 0.912,

respectively. All these comparisons indicate that the B3LYP/6-31G(d) calculation can adequately describe the unique properties of **TS2**.

The CH_3OCO radical has two internal rearrangement pathways. One is the CH_3 migration from the oxygen atom to the carbon atom, forming the CH_3CO_2 radical via a three-membered-ring transition state **TS3**. In **TS3**, the breaking C−O bond and the forming C−C bond are 1.840 and 2.052 Å, respectively. The IRC calculation shows that the C−O bond is elongated continuously and that the C−C bond is shortened simultaneously in the forward direction, resulting in the CH_3CO_2 radical. In the reverse direction, the CH_3OCO radical is formed. Therefore, it is confirmed that **TS3** connects CH_3OCO with the CH_3CO_2 radical. It is noted that Francisco's identification of **TS3** as connecting the CH_3OCO with the final products CH_3 andCO_2 is incorrect. The energy of **TS3** is 38.27 kcal/mol higher than that of the CH_3OCO intermediate. The intermediate CH_3CO_2 (denoted as **IM2**) is 5.54 kcal/mol more stable than **IM1**. The newly formed C−C bond in **IM2** is 1.496 Å with two equal C−O bonds, 1.262 Å.

Starting from **IM2**, two reaction scenarios are possible. One is the direct decomposition of **IM2** to the final products $CH_3 + CO_2$ via transition state **TS4**. As shown in Figure 1, the breaking C−C bond of 1.575 Å is only stretched by 0.079 Å, which indicates that the **TS4** should be very reactant-like, and thus the reaction has an early barrier. The two C−O bonds in the forming CO_2 differ in length by 0.089 Å at the UB3LYP/6-31G(d) level. This C−C bond fission barrier is quite low, i.e., 4.40 kcal/mol. Therefore, the $CH_3 + CO_2$ channel should be the dominant decomposition pathway of **IM2**.

The other minor reaction channel of **IM2** involves the formation of another local minimum, CH_2COOH (**IM3**), via a 1,3-H shift transition state **TS5**. The barrier for this isomerization channel is 31.17 kcal/mol, which is 26.77 kcal/mol higher than that of **TS4**. **TS5** shows a planar four-membered-ring structure with C_s symmetry and a $^2A'$ electronic state. The breaking C−H bond and the forming O−H bond are 1.391 and 1.274 Å, respectively. One of the C−O bonds in **TS5** is shortened by 0.062 Å and the other is elongated by 0.093 Å. The IRC calculation shows that **TS5** links the **IM2** reactant and the **IM3′** product, which has C_s symmetry and a $^2A'$ state. In **IM3′**, two equal C−H bonds are reflected by the HCCO plane. However, **IM3′** has an imaginary frequency of 315 cm^{-1}, which corresponds to the internal rotation of two C−H bonds around the C−C axis. Following this imaginary vibrational mode, the intermediate **IM3** is formed. **IM3** also has C_s symmetry in the $^2A''$ ground state with two in-plane C−H bonds. Both **IM3** and **IM3′** have C═O double-bond-like structure and C−C single-bond-like structure where the unpaired electron is localized at the C atom of the CH_2 group. We did find an electronically excited structure **IM3″** ($\tilde{A}^2A'$), which involves a C═C double bond and a longer C−O single bond. The energy of **IM3″** is 39.38 kcal/mol higher than that of **IM3** at the G2(B3LYP/MP2/CC) level.

IM3 is the most stable intermediate in the $CH_3O + CO$ reaction. The decomposition of **IM3** to $OH + CH_2CO$ is highly endothermic by 47.54 kcal/mol, while the overall reaction is also endothermic by 20.84 kcal/mol. This C−O bond cleavage process is found to be barrierless at the G2(B3LYP/MP2/CC) level. The other possible decomposition pathway of **IM3** resulting in $CH_2(^3B_1) + HOCO(^2A')$ is also highly endothermic by 99.9 kcal/mol and thus is unfavorable. So **IM3** can be treated as a possible final radical product in the $CH_3O + CO$ reaction.

The other rearrangement pathway of **IM1** involves the four-center 1,3-H shift transition state **TS6**. One of the H atoms in the CH_3 group migrates to the other C atom, forming the isomer CH_2OCHO (denoted as **IM4**). The energy of **TS6** is 40.02 kcal/mol higher than that of the **IM1**, which is slightly higher than the CH_3-shift transition state **TS3**. **TS6** has C_s symmetry and a $^2A'$ electronic state. The breaking C−H bond is 1.454 Å, and the forming H−C bond is 1.385 Å. This isomerization path of **IM1** possesses the highest barrier in this study. The isomer **IM4** has no element of symmetry and is 4.40 kcal/mol less stable than **IM1**.

IM4 can dissociate subsequently by the O−C bond cleavage via transition state **TS7** and gives the final reaction products CH_2O and HCO. In **TS7**, the breaking O−C bond is elongated by 0.563 Å, which implies that this transition state has a rather late character. The other C−O bond is shortened by 0.122 Å, forming the CH_2O molecule. This reaction channel is endothermic by 15.35 kcal/mol at the G2(B3LYP/MP2/CC) level. The corresponding barrier height is calculated to be 31.12 kcal/mol. The overall reaction is also slightly endothermic by 4.75 kcal/mol.

B. Direct Abstraction Mechanism. The $CH_3O + CO$ reaction is found to have a direct hydrogen abstraction channel. One of the hydrogen atoms in CH_3O is abstracted by the carbon atom in CO, forming the final products CH_2O and HCO. The transition state involved is shown as **TS8** in Figure 1. **TS8** has C_s symmetry and a $^2A'$ electronic state. The breaking C−H bond is elongated to 1.435 Å. The forming H−C bond is 1.360 Å, which is 0.232 Å longer than the equilibrium C−H bond in the HCO radical. The C−H−C structure is almost linear with an angle of 170.6°. The barrier height for this abstraction path is calculated to be 24.19 kcal/mol, which is 17.80 kcal/mol higher than that for the path of CH_3O addition to CO.

C. Summary of Reaction Mechanism. The profile of the potential energy surface for the most important channels of the $CH_3O + CO$ reaction is shown in Figure 2. The other product channels can be ruled out because of their high endothermicities (e.g., 73.2 and 81.6 kcal/mol relative to the reactants for the $CH_2 + HOCO$ and $O + CH_3CO$ channels, respectively). According to the energetics calculated at the G2(B3LYP/MP2/CC) level, the most favorable pathways leading to the only exothermic products, $CH_3 + CO_2$, can be summarized as follows:

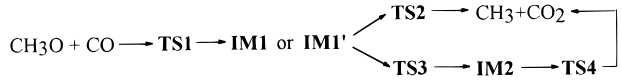

The rate-determining steps for these two channels are decomposition or isomerization of **IM1** or **IM1′**. The products, CH_2O and HCO, can also be formed through two paths. One is the addition−elimination mechanism: $CH_3O + CO \rightarrow$ **TS1** $\rightarrow$ **IM1′** $\rightarrow$ **TS6** $\rightarrow$ **IM4** $\rightarrow$ **TS7** $\rightarrow CH_2O + HCO$. The other is the direct abstraction channel via the transition state **TS8**. Another radical product, CH_2COOH, which is 26.70 kcal/mol more stable than the reactants, is produced by the rearrangement of the CH_3CO_2 radical.

It is worth noting that two new radicals are formed in the reaction process, i.e., CH_3OCO (**IM1**) and CH_3CO_2 (**IM2**), which are analogous to the HOCO and HCO_2 radicals, respectively. Their vibrational frequencies are listed in Table 1. The enthalpies of formation at 0 K, $\Delta H^0_{f,0}$, are calculated to be −36.8 and −42.3 kcal/mol for the CH_3OCO and CH_3CO_2 radicals, respectively, where the $\Delta H^0_{f,0}$ for CH_3OCO is in good agreement with the value of -37.3 ± 3 kcal/mol calculated by Francisco[13] at the G2 level.

2. Multichannel RRKM Calculations of the Rate Constants. We have calculated the rate constants for the formation of various products according to the following reactions:

$$\begin{aligned}
CH_3O + CO \underset{2}{\overset{1}{\rightleftharpoons}} CH_3OCO^* &\xrightarrow{3} CH_3 + CO_2 \\
&\underset{5}{\overset{4}{\rightleftharpoons}} CH_3CO_2^* \xrightarrow{6} CH_3 + CO_2 \\
&\xrightarrow{7} CH_2COOH \\
&\xrightarrow[w_2]{[M]} CH_3CO_2 \\
&\underset{9}{\overset{8}{\rightleftharpoons}} CH_2OCHO^* \xrightarrow{10} CH_2O + HCO \\
&\xrightarrow[w_3]{[M]} CH_2OCHO \\
&\xrightarrow[w_1]{[M]} CH_3OCO \\
CH_3O + CO &\xrightarrow{11} CH_2O + HCO
\end{aligned}$$

where "*" represents the vibrational excitation of the intermediates.

Steady-state assumption for all excited intermediates leads to the following expressions for the second-order rate constants of various product channels:

$$k_{CH_3}(T) = \frac{\alpha_1}{h}\frac{Q_t^{\ddagger}Q_r^{\ddagger}}{Q_{CH_3O}Q_{CO}} e^{-E_1/(kT)} \times \int_0^{\infty} \frac{k_3(E) + X_2(E)\, k_6(E)}{Y(E)} W_1(E^{\ddagger})\, e^{-E^{\ddagger}/(kT)}\, dE^{\ddagger} \quad (1)$$

$$k_{CH_2COOH}(T) = \frac{\alpha_1}{h}\frac{Q_t^{\ddagger}Q_r^{\ddagger}}{Q_{CH_3O}Q_{CO}} e^{-E_1/(kT)} \times \int_0^{\infty} \frac{X_2(E)\, k_7(E)}{Y(E)} W_1(E^{\ddagger})\, e^{-E^{\ddagger}/(kT)}\, dE^{\ddagger} \quad (2)$$

$$k^a_{CH_2O}(T) = \frac{\alpha_1}{h}\frac{Q_t^{\ddagger}Q_r^{\ddagger}}{Q_{CH_3O}Q_{CO}} e^{-E_1/(kT)} \times \int_0^{\infty} \frac{X_3(E)\, k_{10}(E)}{Y(E)} W_1(E^{\ddagger})\, e^{-E^{\ddagger}/(kT)}\, dE^{\ddagger} \quad (3)$$

$$k_{w_1}(T) = \frac{\alpha_1}{h}\frac{Q_t^{\ddagger}Q_r^{\ddagger}}{Q_{CH_3O}Q_{CO}} e^{-E_1/(kT)} \int_0^{\infty} \frac{w_1}{Y(E)} W_1(E^{\ddagger})\, e^{-E^{\ddagger}/(kT)}\, dE^{\ddagger} \quad (4)$$

$$k_{w_2}(T) = \frac{\alpha_1}{h}\frac{Q_t^{\ddagger}Q_r^{\ddagger}}{Q_{CH_3O}Q_{CO}} e^{-E_1/(kT)} \times \int_0^{\infty} \frac{X_2(E)\, w_2}{Y(E)} W_1(E^{\ddagger})\, e^{-E^{\ddagger}/(kT)}\, dE^{\ddagger} \quad (5)$$

$$k_{w_3}(T) = \frac{\alpha_1}{h}\frac{Q_t^{\ddagger}Q_r^{\ddagger}}{Q_{CH_3O}Q_{CO}} e^{-E_1/(kT)} \times \int_0^{\infty} \frac{X_3(E)\, w_3}{Y(E)} W_1(E^{\ddagger})\, e^{-E^{\ddagger}/(kT)}\, dE^{\ddagger} \quad (6)$$

where

$$k_i(E) = \alpha_i C_i\, W_i(E_i^{\ddagger})/N_j(E_j) \quad (7)$$

$$Y(E) = X_1(E) - X_2(E)\, k_5 - X_3 k_9 \quad (8)$$

$$X_1(E) = k_2(E) + k_3(E) + k_4(E) + k_8(E) + w_1 \quad (9)$$

$$X_2(E) = k_4(E)/[k_5(E) + k_6(E) + k_7(E) + w_2] \quad (10)$$

$$X_3(E) = k_8(E)/[k_9(E) + k_{10}(E) + w_3] \quad (11)$$

and

$$w = \beta_c Z_{LJ}[M] \quad (12)$$

In the above equations, α_i is the statistical factor for the ith reaction path and E_1 is the energy barrier for the formation of the CH_3OCO radical via step 1. Q_{CH_3O} and Q_{CO} are the total partition functions of CH_3O and CO, respectively. $Q_t^{\ddagger}$ and $Q_r^{\ddagger}$ are the translational and rotational partition functions of the association **TS1**, respectively. $W_1(E^{\ddagger})$ is the sum of states of **TS1** with excess energy $E^{\ddagger}$ above the association barrier. $k_i(E)$ is the energy-specific rate constant for the ith channel, and C_i is the ratio of the overall rotational partition function of the **TS***i* (i = 2, 3, 4, 5, 6, 7, 8, 9, 10) and the intermediate **IM***j* (j = 1, 2, 4). Because several structures have one small vibrational frequency below 100 cm^{-1}, as shown in Table 1, in the multichannel RRKM calculations, we have substituted this low-frequency vibration by free rotation around a suitable axis. The reduced moment of inertia for the free rotation was computed from the optimized geometry and is listed in Table 1. Because all the transition states are tight, the sum of states $W_i(E_i^{\ddagger})$ was calculated by the convolution of the vibrational and rotational sum of states counted with the extended Beyer−Swinehart algorithm.[24,25] $N_j(E_j)$ is the density of states at the energy E_j of the intermediate **IM***j*. w_j is the effective collision frequency for the jth intermediate. β_c is the collision efficiency that is calculated using Troe's weak-collision approximation.[26] Z_{LJ} is the Lennard-Jones collision frequency, and [M] is the concentration of the bath gas M. However, since the Lennard-Jones parameters for the molecules involved in all the reaction paths are not available in the literature, the estimated data, ϵ = 200 K and σ = 5.0 Å, were used in the calculation. Furthermore, we assumed that the collision frequency factor Z_{LJ} is the same for all the intermediates.[27]

The rate constants for the direct abstraction of CH_3O by CO can be obtained readily using the conventional transition-state theory:[28]

$$k_{Abs}(T) = \alpha\frac{kT}{h}\frac{Q_{TS8}^{\ddagger}}{Q_{CH_3O}Q_{CO}} e^{-E_a/(kT)} \quad (13)$$

Because the transition state **TS8** has two low vibrational frequencies, a two-dimensional rotor approximation was used in the calculation.

The total second-order rate constant for the CH_3O + CO reaction is given by

$$k_{tot}(T) = k_{CH_3}(T) + k_{CH_2COOH}(T) + k^a_{CH_2O}(T) + k_{w_1} + k_{w_2} + k_{w_3} + k_{Abs} \quad (14)$$

and the branching ratios symbol γ_i for all the different open channels considered in the reaction are evaluated by

$$\gamma_i = k_i(T)/k_{tot}(T) \quad (15)$$

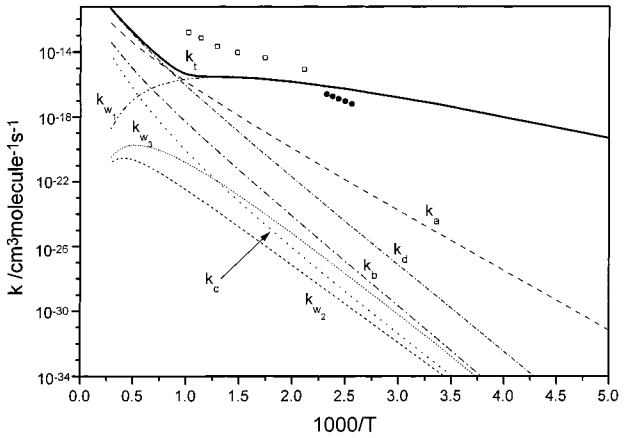

Figure 3. Arrhenius plots of the total and individual rate constants for the CH_3O + CO reaction and its various channels: k_t, total rate constant; k_a, CH_3 + CO_2; k_b, CH_2O + CO; k_c, CH_2COOH; k_d, abstraction channel; k_{w1}, stabilization of **IM1***; k_{w2}, stabilization of **IM2**; k_{w3}, stabilization of **IM4**. [M] = 50 Torr of Ar. Circles designate experimental data from ref 8. Squares show experimental data from ref 11.

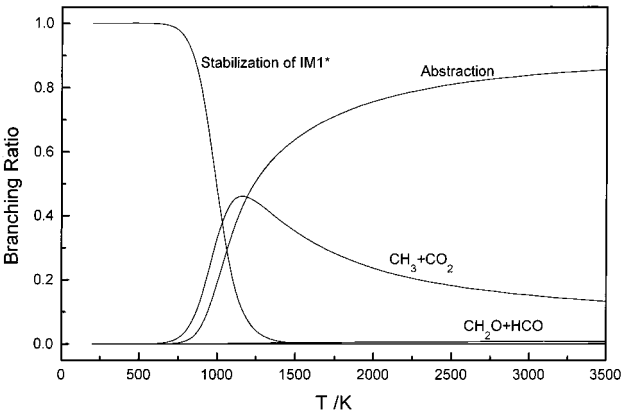

Figure 4. Branching ratios for various products for the CH_3O + CO reaction, which correspond to Figure 3 with a pressure of 50 Torr Ar. Only the deactivation of **IM1**, CH_3 + CO_2, CH_2O + HCO, and the direct abstraction channels are shown because the other channels are negligible.

A. Temperature Dependence. We have performed the RRKM calculations at a pressure of 50 Torr of Ar and compared the predicted values with the experimental data. The total and individual rate constants are shown in Figure 3, and the branching ratios for some channels are depicted in Figure 4. At temperatures below 1000 K, the rate constant is weakly temperature-dependent while the reaction is dominated by the stabilization of the CH_3OCO radical. This is consistent with the experimental observation[9] that the principal reaction product was not CO_2 but $(CH_3O)_2CO$ or $(CH_3OCO)_2$, which results from the secondary reactions of CH_3OCO + CH_3O → $(CH_3O)_2CO$ or CH_3OCO + CH_3OCO → $(CH_3OCO)_2$. At higher temperatures, the rate constant becomes strongly temperature-dependent, which implies that the reaction mechanism has changed. Obviously, the CH_3 + CO_2 channel takes over. Above 1250 K, however, the direct abstraction channel becomes dominant and the CH_3 + CO_2 channel becomes less and less important. So the major products become CH_2O + HCO. Because there is no high-temperature measurements of the CH_3O + CO reaction, this prediction can be a guide for the future experimental observation. Over the temperature range 200−3500 K, the other channels such as CH_2O + HCO from the addition−elimination mechanism and the CH_2COOH radical product do not play any observable role in the CH_3O + CO reaction. It is worth noting that this kinetic behavior of the CH_3O + CO reaction is similar to that of the OH + CO reaction.[5]

TABLE 3: Best-Fit Parameters of the Empirical Expression $k = A\,(T/1000)^n \exp(-E/T)$ for the Rate Constants of the CH_3O + CO Reaction at 200−3500 K and 760 Torr of Air

temperature (K)	ln A^a	n	E^b
200−1000	−28.99 ± 0.06	−4.93 ± 0.18	4570 ± 80
1000−1500	−67.14 ± 0.98	32.17 ± 0.82	−33490 ± 1000
1500−3500	−26.0 ± 0.07	2.28 ± 0.04	10120 ± 90

[a] A in cm^3 $molecule^{-1}$ s^{-1}. [b] In kelvin.

The room-temperature total rate constant is in agreement with the upper limit value estimated by Sander et al.[10] In the temperature range 400−1000 K, the theoretical values lie between the results obtained by Lissi et al.[8] at low temperature and the data obtained by Wantuck et al.[11] at high temperature. It is not surprising that a large difference occurs. Lissi et al.[8] obtained the rate constants by monitoring the rate of CO_2 production during thermal decomposition of dimethyl peroxide in the presence of carbon monoxide. Their results correspond to the k_a in Figure 3. However, in the temperature range they considered, the major channel should be the stabilization of the CH_3OCO radicals. The yield of CO_2 is very minor. Therefore, the large experimental errors may be inevitable. Moreover, their rate constants were determined from the indirect measurements and depend on the values assumed for the reactions CH_3OOCH_3 → $2CH_3O$ and CH_3O + CH_3O → CH_3OH + CH_2O. Consequently, the accuracy of the rate constants may be suspected. On the other hand, Wantuck et al.[11] measured the total rate constant for the sum of all the possible removal paths of CH_3O in the laser photolysis of the CH_3OH + CO + Ar mixture experiment using the LIF technique. It must be noted that the use of the LIF technique to study methoxy radical reactions is limited by rapid quenching of the fluorescence emission. The room-temperature quenching rate constant for the fluorescence emission of $CH_3O(A^2A_1)$ is 10^{-10} cm^3 $molecule^{-1}$ s^{-1}, which is 8 orders of magnitude higher than the reaction rate of CH_3O with CO. Moreover, other removal channels of CH_3O must be involved in their reactor. So we think the data measured by Wantuck et al. can only be considered as the upper limits. Further experiments and analysis are required to fully understand the fundamental rate constant parameters for the CH_3O + CO reaction.

RRKM/TST calculations have also been performed at atmospheric pressure of the bath gas (m = 29) for practical use. The total rate constant can be determined by a least-squares fitting of three parameters of $k = A(T/1000)^n \exp(-E/T)$ over the temperature range 200−3500 K. The best-fit parameters are listed in Table 3.

B. Pressure Dependence. There is no pressure-dependence studies reported previously for the CH_3O + CO reaction. We have performed a priori calculations for the total rate constant and branching ratio over a wide pressure range 10^{-10}−10^{10} Torr at the selected temperatures 300, 500, 1000, 2000, and 3000 K. The results are shown in Figures 5 and 6, respectively.

It is obvious that the rate constants show typical falloff behavior at various temperatures. With the elevation of the temperature, the falloff range shifts to the high pressure. At very low pressure, the production of CH_3 + CO_2 is the major reaction channel. At high pressure, the dominant channel is the stabilization of the CH_3OCO radicals. However, at relatively high temperatures, the direct abstraction channel becomes competitive. All of these theoretical predictions must await future experimental verification.

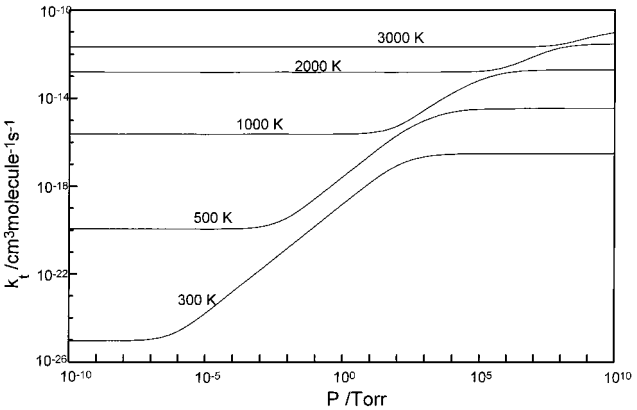

Figure 5. Pressure dependence of the total rate constants for the $CH_3O + CO$ reaction at 300, 500, 1000, 2000, and 3000 K.

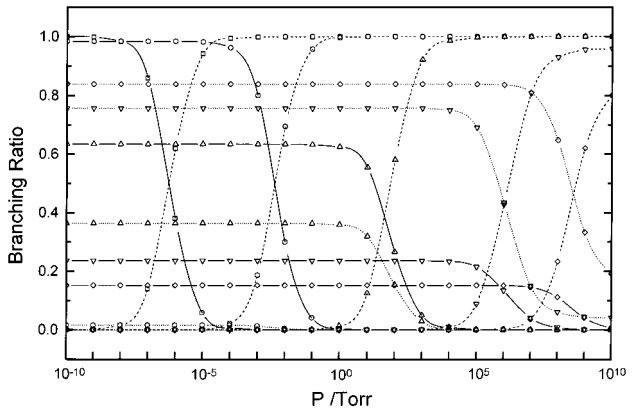

Figure 6. Branching ratios for the $CH_3 + CO_2$ (solid lines), the deactivation of **IM1** (dash lines), and the abstraction channels (dot lines). The squares, circles, up triangles, down triangles, and diamonds represent temperatures of 300, 500, 1000, 2000, and 3000 K, respectively.

C. Tunneling Effect. It is noted that the tunneling effect was not considered in the above kinetic calculations. Because each reaction channel possesses significant energy barriers and because the energy barriers for the addition and the abstraction are well separated, the magnitude of the rate constant will be determined mainly by individual barrier height. In addition, several difficulties prevent us from correcting for the tunneling effect. Most importantly, there is no appropriate method to treat the tunneling effect in our multichannel RRKM calculation. One-dimensional tunneling methods, such as the Wigner method, often prove to be qualitatively incorrect.[29] The other semiclassical approximations, such as the small-curvature tunneling (SCT) and the large-curvature tunneling (LCT) developed by Truhlar et al.,[30,31] may be suitable. Unfortunately, these methods are too complex to be applied in our multichannel RRKM program.

To check the reliability of such a simplification, we have estimated the tunneling effect qualitatively. An asymmetric Eckart potential[32] was used to calculate the tunneling factor $\kappa(T)$. For the addition mechanism, $\kappa(T)$ was always in the range 1.2−1.0 from 200 to 3000 K. For the direct abstraction step, the $\kappa(T)$ is relatively large at the low temperatures. The values of $\kappa(T)$ at 200, 300, and 500 K are 6.7×10^6, 143, and 3.4, respectively. However, this significant tunneling effect cannot influence our kinetic calculations significantly. For example, at 200 K, even if the tunneling correction is included, the dominant channel is still the deactivation of CH_3OCO with a rate of 1.2×10^{-19} cm^3 molecule^{-1} s^{-1} because this value is about 5 orders of magnitude higher than that for the abstraction pathway ($\sim 7.0 \times 10^{-25}$ cm^3 moelcule^{-1} s^{-1}). From 1000 to 3000 K, $\kappa(T)$ is in the range 1.0−1.3. This indicates that the tunneling effect is not significant at higher temperatures.

3. Implications for Atmospheric and Combustion Chemistry. Under typical atmospheric conditions ($T = 250$ K and $P = 5$ Torr), the individual rate constants are 3.16×10^{-28}, 3.11×10^{-37}, 1.03×10^{-35}, 1.39×10^{-19}, 1.60×10^{-38}, 5.74×10^{-37}, and 3.26×10^{-33} (in units of cm^3 molecule^{-1} s^{-1}) for the channels $CH_3 + CO_2$, CH_2COOH, $CH_2O + HCO$, CH_3OCO, CH_3CO_2, CH_2OCHO, and the direct abstraction channel, respectively. It is obvious that the stabilization of CH_3OCO^* dominates the $CH_3O + CO$ reaction. As mentioned above, the abstraction channel still plays a minor role even if the tunneling correction is considered. Meanwhile, the formation of CH_3 and CO_2 is only a very minor channel with a relatively small rate constant.

Under combustion conditions ($T = 2500$ K and $P = 760$ Torr), the individual rate constants are 1.32×10^{-13}, 5.12×10^{-16}, 5.23×10^{-15}, 3.10×10^{-17}, 3.74×10^{-19}, 1.61×10^{-19}, and 5.90×10^{-13} (in cm^3 molecule^{-1} s^{-1}) for the channels $CH_3 + CO_2$, CH_2COOH, $CH_2O + HCO$, CH_3OCO, CH_3CO_2, CH_2OCHO, and the direct abstraction channel, respectively. Therefore, CH_2O and HCO from the abstraction channel are the major products, accounting for a branching ratio of 81%. The minor products are CH_3 and CO_2 with a yield of 18%. The other products are negligible.

IV. Conclusions

The following conclusions can be drawn from this theoretical investigation of the $CH_3O + CO$ reaction.

(1) Two kinds of mechanisms are revealed for the $CH_3O + CO$ reaction. One is the addition of CH_3O with CO via a barrier of 6.39 kcal/mol. The CH_3OCO radical is formed and then decomposes to the final products. The other channel is direct hydrogen abstraction of CH_3O by CO via a barrier of 24.19 kcal/mol, forming CH_2O and HCO.

(2) At lower temperatures, the stabilization of the adduct CH_3OCO dominates the reaction. The rate constant shows a weak temperature dependence. At higher temperatures, the products CH_3 and CO_2 and the abstraction paths become dominant. The rate constant shows a strong temperature dependence.

(3) The title reaction exhibits a strong pressure dependence. Over a wide range of pressures, the total rate constant shows an obvious falloff behavior. The $CH_3O + CO$ reaction should be reexamined in future experiments.

(4) The enthalpies of formation at 0 K, $\Delta H^0_{f,0}$, for two important radicals, CH_3OCO and CH_3CO_2, are calculated to be −36.8 and −42.3 kcal/mol, respectively.

(5) Under typical atmospheric conditions, the $CH_3O + CO$ reaction is very slow and the major product should be the CH_3OCO radical. The product yields of CH_3 and CO_2 are very minor. However, under combustion conditions, the major products become CH_2O and HCO.

Acknowledgment. The authors express their gratitude to Dr. A. Vahid for his careful checking and improvement of the English of manuscript.

References and Notes

(1) Aikin, A. C. *J. Geophys. Res.* **1982**, *87*, 3105.

(2) Atkinson, R.; Lloyd, A. C. *J. Phys. Chem. Ref. Data* **1984**, *13*, 315.

(3) Perner, D.; Platt, U.; Trainer, M.; Hubler, G.; Drummond, J.; Junkermann, W.; Rudolph, J.; Schubert, B.; Volz, A.; Elhalt, D. H. *J. Atmos. Chem.* **1987**, *5*, 185.

(4) Heicklen, H.; Westberg, K.; Cohen, N. *The Conversion of NO to NO_2 in Polluted Atmospheres*; Publication No. 115-169; The Pennsylvania State University Center for Air Environment Studies, PA, 1969.
(5) Kudla, K.; Schatz, G. C.; Wagner, A. F. *J. Chem. Phys.* **1991**, *95*, 1635.
(6) Baulch, D. L.; Cobos, C. J.; Cox, R. A.; Esser, C.; Frank, P.; Just, Th.; Kerr, J. A.; Pilling, M. T.; Troe, J.; Walker, R. W.; Warnatz, J. *J. Phys. Chem. Ref. Data* **1992**, *21*, 411.
(7) Steinfeld, J. I.; Francisco, J. S.; Hase, W. L. *Chemical Kinetics and Dynamics*; Prentice-Hall: Englewood Cliffs, NJ, 1989.
(8) Lissi, E. A.; Massiff, G.; Villa, A. E. *J. Chem. Soc., Faraday Trans. 1* **1973**, *69*, 346.
(9) Wiebe, H. A.; Heicklen, J. *J. Am. Chem. Soc.* **1973**, *95*, 1.
(10) Sanders, N.; Butler, J. E.; Pasternack, L. R.; McDonald, J. R. *Chem. Phys.* **1980**, *49*, 17.
(11) Wantuck, P. J.; Oldenborg, R. C.; Baughcum, S. L.; Winn, K. R. *Chem. Phys. Lett.* **1987**, *138*, 548.
(12) Mebel, A. M.; Diau, E. W. G.; Lin, M. C.; Morokuma, K. *J. Am. Chem. Soc.* **1996**, *118*, 9759.
(13) Francisco, J. S. *Chem. Phys.* **1998**, *237*, 1.
(14) Bauschlicher, C. W.; Partridge, H. *J. Chem. Phys.* **1995**, *103*, 1788.
(15) Becke, A. D. *J. Chem. Phys.* **1993**, *98*, 5648.
(16) Lee, C.; Yang, W.; Parr, R. G. *Phys. Rev.* **1988**, *B37*, 785.
(17) Gonzalez, C.; Schlegel, H. B. *J. Phys. Chem.* **1989**, *90*, 2154.
(18) Curtiss, L. A.; Raghavachari, K.; Trucks, G. W.; Pople, J. A. *J. Chem. Phys.* **1993**, *98*, 1293.
(19) Frisch, M. J.; Trucks, G. W.; Schlegel, H. B.; Gill, P. W. M.; Johnson, B. G.; Robb, M. A.; Cheeseman, J. R.; Keith, T. A.; Petersson, G. A.; Montgomery, J. A.; Raghavachari, K.; Allaham, M. A.; Zakrzewski, V. G.; Ortiz, J. V.; Foresman, J. B.; Cioslowski, J.; Stefanov, B. B.; Nanayakkara, A.; Challacombe, M.; Peng, C. Y.; Ayala, P. Y.; Chen, W.; Wong, M. W.; Andres, J. L.; Replogle, E. S.; Gomperts, R.; Martin, R. L.; Fox, D. J.; Binkley, J. S.; Defrees, D. J.; Baker, J.; Stewart, J. P.; Head-Gordon, M.; Gonzales, C.; Pople, J. A. *Gaussian 94*; Gaussian Inc.: Pittsburgh, PA, 1995.
(20) Diau, E. W. G.; Lin, M. C.; Melius, C. F. *J. Chem. Phys.* **1994**, *101*, 3923.
(21) Berman, M. R.; Lin, M. C. *J. Phys. Chem.* **1983**, *87*, 3933.
(22) Hsu, D. S. Y.; Snaub, W. M.; Creamer, T.; Gutman, D.; Lin, M. C. *Ber. Bunsen-Ges. Phys. Chem.* **1983**, *87*, 909.
(23) Baulch, D. L.; Cox, R. A.; Hampson, R. F.; Kerr, J. A., Jr.; Troe, J.; Waston, R. T. *J. Phys. Chem. Ref. Data* **1980**, *9*, 466.
(24) Stein, S. E.; Rabinovitch, B. S. *J. Chem. Phys.* **1973**, *58*, 2438.
(25) Astholz, P. G.; Troe, J.; Wieters, W. *J. Chem. Phys.* **1979**, *70*, 5107.
(26) Troe, J. *J. Chem. Phys.* **1977**, *66*, 4745.
(27) Marchand, N.; Rayez, J. C.; Smith, S. C. *J. Phys. Chem. A* **1998**, *102*, 3358.
(28) Smith, I. W. M. *Kinetics and Dynamics of Elementary Gas Reactions*; Butterworth: London, 1980; p 118.
(29) Lu, D. H.; Maurice, D.; Truhlar, D. G. *J. Am. Chem. Soc.* **1990**, *112*, 6206.
(30) Liu, Y. P.; Lynch, G. C.; Truong, T. N.; Lu, D. H.; Truhlar, D. G.; Garrett, B. C. *J. Am. Chem. Soc.* **1993**, *115*, 2408.
(31) Liu, Y. P.; Lu, D. H.; Gonzalez-Lafont, A.; Truhlar, D. G.; Garrett, B. C. *J. Am. Chem. Soc.* **1993**, *115*, 7806.
(32) Johnston, H. S.; Heicklen, J. *J. Chem. Phy.* **1962**, *66*, 532.